

Tropopause and hygropause variability over the equatorial Indian Ocean during February and March 1999

A. R. MacKenzie,¹ C. Schiller,² T. Peter,³ A. Adriani,^{4,5} J. Beuermann,^{2,6} O. Bujok,^{2,7} F. Cairo,^{4,8} T. Corti,³ G. DiDonfrancesco,⁹ I. Gensch,² C. Kiemle,¹⁰ M. Krämer,² C. Kröger,^{1,11} S. Merkulov,¹² A. Oulanosky,¹² F. Ravegnani,^{13,14} S. Rohs,² V. Rudakov,¹² P. Salter,^{15,16} V. Santacesaria,^{17,18} L. Stefanutti,^{17,19} and V. Yushkov¹²

Received 7 September 2005; revised 27 March 2006; accepted 23 May 2006; published 30 September 2006.

[1] Measurements of temperature, water vapor, total water, ozone, and cloud properties were made above the western equatorial Indian Ocean in February and March 1999. The cold-point tropopause was at a mean pressure-altitude of 17 km, equivalent to a potential temperature of 380 K, and had a mean temperature of 190 K. Total water mixing ratios at the hygropause varied between 1.4 and 4.1 ppmv. The mean saturation water vapor mixing ratio at the cold point was 3.0 ppmv. This does not accurately represent the mean of the measured total water mixing ratios because the air was unsaturated at the cold point for about 40% of the measurements. As well as unsaturation at the cold point, saturation was observed above the cold point on almost 30% of the profiles. In such profiles the air was saturated with respect to water ice but was free of clouds (i.e., backscatter ratio <2) at potential temperatures more than 5 K above the tropopause and hygropause. Individual profiles show a great deal of variability in the potential temperatures of the cold point and hygropause. We attribute this to short timescale and space-scale perturbations superimposed on the seasonal cycle. There is neither a clear and consistent “setting” of the tropopause and hygropause to the same altitude by dehydration processes nor a clear and consistent separation of tropopause and hygropause by the Brewer-Dobson circulation. Similarly, neither the tropopause nor the hygropause provides a location where conditions consistently approach those implied by a simple “tropopause freeze drying” or “stratospheric fountain” hypothesis.

Citation: MacKenzie, A. R., et al. (2006), Tropopause and hygropause variability over the equatorial Indian Ocean during February and March 1999, *J. Geophys. Res.*, *111*, D18112, doi:10.1029/2005JD006639.

1. Introduction

[2] The stratosphere can be considered to consist of two, very different, regions: the “overworld,” with a lower boundary given by the first potential temperature, θ , surfaces to lie entirely within the stratosphere (~ 380 K), and the “middleworld” or “lowermost stratosphere,” which lies between the overworld and the tropopause [Holton *et al.*,

1995]. The lowermost stratosphere experiences considerable interchange of air with the troposphere; this interchange being driven by synoptic-scale eddies and folds [e.g., Dethof *et al.*, 2000]. In contrast, the movement of air through the stratospheric overworld is driven by a slow meridional motion, the Brewer-Dobson circulation. Air enters the overworld primarily in the tropics [Brewer,

¹Environmental Science Department, Lancaster University, Lancaster, UK.

²Institute for Stratospheric Research, Forschungszentrum Jülich GmbH, Jülich, Germany.

³Institute for Atmospheric and Climate Science, Swiss Federal Institute of Technology, Zurich, Switzerland.

⁴Institute for Atmospheric Physics, Consiglio Nazionale delle Ricerche, Rome, Italy.

⁵Now at Istituto di Fisica dello Spazio Interplanetario, Consiglio Nazionale delle Ricerche, Frascati, Italy.

⁶Now at Eurofins Hamburg, Hamburg, Germany.

⁷Now at VDI Technologiezentrum, GmbH, Dusseldorf, Germany.

⁸Now at Istituto di Scienze dell’Atmosfera e del Clima, Consiglio Nazionale delle Ricerche, Rome, Italy.

⁹Ente per le Nuove Tecnologie, l’Energia, el’Ambiente, Casaccia, Rome, Italy.

¹⁰Arbeitsgruppe Lidar, Institut für Physik der Atmosphäre, Deutsches Zentrum für Luft- und Raumfahrt Oberpfaffenhofen, Wessling, Germany.

¹¹Now at National Isotope Centre Institute of Geological and Nuclear Science, Lower Hutt, New Zealand.

¹²Central Aerological Observatory, Dolgoprudny, Russia.

¹³Luigi Foschini Institute, Consiglio Nazionale delle Ricerche, Bologna, Italy.

¹⁴Now at Istituto di Scienze dell’Atmosfera e del Clima, Consiglio Nazionale delle Ricerche, Bologna, Italy.

¹⁵Met Office, Exeter, UK.

¹⁶Retired.

¹⁷Airborne Platform for Earth Observation, Comitato di Gestione, Florence, Italy.

¹⁸Now at Advanced Computer Systems, SpA, Rome, Italy.

¹⁹Now at Geophysica Gruppo Europeo di Interesse Economico, Florence, Italy.

1949]. This air has well-defined concentrations of trace gases with long tropospheric lifetimes (the CFCs, for example) but has much less well-defined concentrations of compounds with short tropospheric (chemical or physical) lifetimes, including water vapor. Water vapor is important in stratospheric chemistry as a source of HO_x radicals and as the major condensate in polar stratospheric clouds, and it plays an essential role in the stratospheric radiation budget [e.g., *Dvortsov and Solomon*, 2001; *Forster and Shine*, 1999].

[3] The observed increase of water vapor in the stratosphere over the last decades cannot be explained quantitatively by the atmospheric increase of methane alone [e.g., *Rosenlof et al.*, 2001]. Considerable drying takes place as air moves from troposphere to stratosphere in the tropics. The only plausible mechanism for such drying is “freeze-drying”: the cooling of a cloud-laden air parcel to the temperature at which the local saturation mixing ratio is less than or equal to the observed stratospheric water vapor mixing ratio (to be precise, that part of the observed stratospheric mixing ratio not due to methane oxidation). The excess water, condensed in the cloud elements, is then assumed to sediment from the air parcel in the form of ice crystals.

[4] Several hypotheses have been put forward to explain where and how drying of air entering the stratosphere occurs. The “stratospheric fountain” hypothesis of *Newell and Gould-Stewart* [1981] suggests that (1) cross-tropopause transport occurs predominantly over Indonesia and the maritime continent in northern winter, and over northern India in northern summer and that (2) large-scale layers of subvisible cirrus occur over these regions at these times. The detection of large-scale subvisible cirrus layers in the tropics [*Wang et al.*, 1996] and the results of trajectory-based studies [*Fueglistaler et al.*, 2004; *Bonazzola and Haynes*, 2004] have rekindled interest in versions of this hypothesis. *Holton and Gettelman* [2001] suggested that horizontal transport through this cold trap region brings very dry air to other longitudes where it can finally be transported into the stratosphere. Recent trajectory studies using 21 years of reanalyses from the ERA-40 data of the European Centre for Medium-Range Weather Forecasting (ECMWF) have shown that fixing the final water vapor mixing ratio in a trajectory to that given by the saturation mixing ratio at the coldest temperature along the trajectory gives a satisfactory fit to long-term average stratospheric humidity and to the seasonal cycle [*Fueglistaler et al.*, 2005].

[5] *Danielsen* [1982] proposed an alternative based on the dynamics of individual convective clouds: that tropical convective clouds penetrate the tropopause. Radiatively driven overturning of the thick cirrus anvils from the convection then allows cloud particles to grow sufficiently that they sediment out, thus drying the air. There have been a few observations of this mechanism apparently at work [*Danielsen*, 1993]. It is not clear if there is sufficient tropopause-penetrating convection to allow the Danielsen mechanism alone to dry all the air moving into the stratospheric overworld, as forced by the Brewer-Dobson circulation. Convective cloud at the tropical tropopause implies air masses that are very different from their surroundings (i.e., with trace gas and total water signatures indicative

of rapid diabatic transport (convection) rather than cloud formation in situ). Such signatures would include low mixing ratios of ozone, high mixing ratios of total water, and localized ice supersaturation within the cloudy air mass (since cloud formation took place at lower altitudes).

[6] A third hypothesis requires active convection, but not tropopause penetration. *Potter and Holton* [1995] postulate convectively induced gravity waves in the lower stratosphere as a source of adiabatic cooling, cloud formation, and, thence, dehydration. Another possible source of adiabatic cooling is from planetary wave activity, such as Kelvin waves [*Jensen et al.*, 1996]. In situ cloud formation at the tropical tropopause implies air masses that are similar to their surroundings (i.e., with trace gas and total water signatures indicative of adiabatic rather than diabatic transport). Such signatures would include average mixing ratios of ozone, average mixing ratios of total water, and ice supersaturation that is not restricted to the cloudy air mass (since cloud formation in the upper troposphere appears to require substantial supersaturation).

[7] A fourth hypothesis [*Sherwood and Dessler*, 2000] combines the overshooting dehydration of *Danielsen* [1993] with slow upward motion through a thick tropopause layer. The existence of a tropopause layer several kilometers thick has been suggested at various times in the literature (see the review in *Highwood and Hoskins* [1998]). The tropopause layer is sometimes referred to as the substratosphere, since it is above the mean level of tropospheric convection [*Thuburn and Craig*, 2002]. It is also known as the tropical tropopause transition layer (TTL), a region that is not efficiently flushed by convection and that, for the most part, is subject to radiative heating [*Folkins et al.*, 1999].

[8] Analysis of data obtained at different tropical stations and seasons show, that the relative contribution of the aforementioned dehydration processes varies with longitude and season [*Vömel et al.*, 2002]. However, in that study, deep convection was found to be important only in setting up the tropical tropopause layer which is then subject to large-scale wave activity and wave breaking at the tropopause. In general, progress in distinguishing the effectiveness of the different dehydration mechanisms has been slow, due to the sparseness of observations, particularly coincident observations of temperature, humidity, water vapor, condensed water, and gas-phase tracers of atmospheric transport.

[9] During February and March 1999, the European Airborne Platform for Earth Observation–Third European Stratospheric Experiment on Ozone (APE-THESEO) mission took place, based on Mahé on the Seychelles (4°42'S, 55°30'E) in the Indian Ocean, where the UTLS region had not been the target of a major scientific campaign involving aircraft or balloons before. For this project, the Russian high-altitude research aircraft *Geophysica* was equipped with a comprehensive in situ payload, accompanied by the DLR *Falcon* carrying a lidar and radiometers, which acted as a pathfinder for cloud studies with the *Geophysica*. Flight paths consisted of a combination of long-range transects, nominally directed normal to the intertropical convergence zone (ITCZ), and more complicated interceptions of cloud systems.

[10] APE-THESEO aimed to study the transport, chemistry, and cloud physics of the tropical tropopause region

[MacKenzie *et al.*, 2000; Stefanutti *et al.*, 2004], particularly with respect to factors affecting the concentrations of trace gases in the stratosphere. Below, we use the data collected during APE-THESEO, along with radiosonde and meteorological analyses, to describe the structure and variability of the tropopause over the equatorial Indian Ocean during northern winter/spring 1999. A summary of the characteristics of all the ascents and descents across the tropopause, made during the campaign, is given first. Individual profiles are then discussed in detail, in the light of the hypotheses above. Finally, the mean water vapor profile is compared to mean profiles from previous aircraft missions and discussed in terms of the tropical “tape recorder” paradigm. A previous analysis of the total water data used below can be found in the work of *Beuermann* [2000].

2. Instruments and Data

[11] The following analysis uses in situ data of water (total and vapor), ozone and particles, measured from the *Geophysica* aircraft [Stefanutti *et al.*, 1999] over the Indian Ocean in February and March 1999. We also use routine measurements of temperature, pressure, position, etc., from the aircraft sensors.

[12] The Fast In situ Stratospheric Hygrometer (FISH), developed at the Forschungszentrum Jülich (Germany), is based on the Lyman α photofragment fluorescence technique. It has flown previously on other aircraft [Zöger *et al.*, 1999]. The overall accuracy of this hygrometer is 6%, or 0.3 ppmv in the case of the very low mixing ratios that occur in the tropics. FISH was shown to yield results that are consistent with other stratospheric water vapor measurements [Kley *et al.*, 2000]. In the presence of clouds, FISH measures total water, with an oversampling of cloud elements [Schiller *et al.*, 1999]. For typical *Geophysica* cruising altitude and speed, the oversampling factor for particles with radii larger than 4 μm is 5. Thus FISH measurements are very sensitive to cloud water content.

[13] The Fluorescent Airborne Stratospheric Hygrometer FLASH instrument developed by the Central Aerological Observatory (Moscow) is an aircraft version of the water vapor instrument that has previously been deployed on balloon [Merkulov and Yushkov, 1999], and also uses the Lyman α fluorescence technique. During APE-THESEO, the inlet was designed to measure gas-phase water providing complementary information to the FISH total water measurement inside clouds. Out of cloud, FISH and FLASH gave generally consistent data. Since FISH was calibrated between all flights during APE-THESEO, and FLASH only once before the campaign, for this study FLASH was recalibrated against FISH during out-of-cloud measurements.

[14] Temperature on board the *Geophysica* aircraft during the APE-THESEO campaign was measured by the onboard system whose accuracy is specified to ± 0.5 K (B. Lepouchov, Myasishchev Design Bureau, Russia, personal communication, 2000). Comparison with independent temperature probes (Rosemount TDC probe, microwave temperature profiler) available on this aircraft during following projects confirmed this accuracy. For the RHi calculated in the discussion chapter (in particular, Figure 7),

this uncertainty translates in an uncertainty of approximately $\pm 15\%$ RHi, assuming 3 ppmv H_2O mixing ratio and conditions close to saturation.

[15] The Electro-Chemical Ozone Cell (ECOC) is a modified electrochemical ozonesonde. Ozone measurements from ECOC have been validated against ozonesondes [Kyrö *et al.*, 2000] and shown to yield a small negative bias of $-5.7 \pm 2.8\%$. Such a bias is not significant in the context of the following analysis. Fast Ozone Analyzer (FOZAN) is a chemiluminescent ozone sensor [Yushkov *et al.*, 1999] based on a solid-phase dye. FOZAN can detect fast ozone variations, but needs frequent calibration, and ECOC has been used as a reference instrument for the FOZAN. In flights where both ECOC and FOZAN were operating, ECOC and FOZAN showed generally close agreement, with an average correlation coefficient of 0.94 and no significant bias. Here we use ECOC data throughout except for the last scientific sortie (11 March 1999) when they are absent and FOZAN data are used in their place.

[16] The Multiwavelength Aerosol Laser Scatterometer (MAS) first flew on the *Geophysica* during the APE-POLECAT mission [Adriani *et al.*, 1999]. In daylight, MAS measures backscatter and depolarization at 532 nm. The Sun is required to be outside the field of view of the instrument (i.e., a solid angle of 20°), looking horizontally through a shutter on the starboard side of the aircraft. Since sorties were often conducted around sunrise, there were several occasions when the MAS shutter was closed to prevent direct sunlight entering the instrument.

[17] Besides MAS there was other in situ cloud and aerosol instrumentation on board the *Geophysica* (FSSP-300, Mini Copas, CVI). Descriptions can be found in the work of Stefanutti *et al.* [2004]. We do not present data from these instruments here, but we do draw on the analysis of FSSP data given by Thomas *et al.* [2002]. The in situ measurements from the *Geophysica* are complemented by lidar observations of clouds and aerosols from the *Falcon* aircraft. A recent description of the lidar is given by Flentje *et al.* [2002].

3. Results

[18] During APE-THESEO, 11 flights of the *Geophysica* aircraft were carried out in the tropical region over the Indian Ocean providing 37 individual vertical profile observations. Details of the locations of the profiles are given in Table 1. The first of these profiles was obtained at 31°N , and so, strictly, outside the tropics. Some of the flight legs included long periods of horizontal flight or slow climbs, so that some of the vertical sections are composed of data taken over a wide area (as short as 250 km and as long as 2000 km). The vertical profiles taken over a long duration did not show any systematic difference to those taken over a shorter duration. Nevertheless, these aircraft-derived vertical profiles should not be overinterpreted, because the air masses at different altitudes have only a limited common history as a result of vertical shear in the horizontal winds. This implies, inter alia, lower correlations between measures of TTL structure with increasing vertical separation.

[19] We determined for all tropical ascents and descents of the campaign the cold-point tropopause, the lapse-rate tropopause, and the highest pressure-altitudes, where 100

Table 1. Individual Profiles Measured by the *Geophysica* During APE-THESEO^a

Day	Time	UCSE					FISH					Z _{CT}
		Lat.	T _{cp}	Z _{cp}	θ _{cp}	e _{cp}	χ _H	Z _H	e _H	Z _{CT}		
1	13 Feb 1999	48–49.4	31	202	17.3	411	28.3	4.8	16.4	45.6	ND	
2		60–62	12	190	17.4	389	4.1	2.4	17.6	4.7	ND	
3	14 Feb 1999	29–31	10	187	18.4	401	3.0	4.1	18.4	3.0	ND	
4		40–43.8	–4	187	17.2	379	2.5	2.1	17.7	3.4	ND	
5	19 Feb 1999	35–39	–3	184	17.7	380	1.4	3.5	17.6	1.4	17.3	
6		39–41.5	0	183	18.1	386	1.4	2.0	18.1	1.5	18.0	
7		41.5–45	–2	182	18.1	383	1.1	1.6	18.1	1.1	18.1	
8		45–48.5	–2	185	17.5	379	1.6	1.8	17.5	1.6	17.7	
9		48.5–52.3	–6	187	17.9	392	2.8	1.8	17.4	3.1	ND	
10	24 Feb 1999	20.7–23	–8	188	17.4	383	2.6	2.6	17.6	3.9	14.8	
11		23–28.4	–7	189	16.8	377	3.2	2.3	17.2	3.8	ND	
12	27 Feb 1999	10.3–24	–10	188	16.7	373	2.7	1.5	17.2	6.5	15.6	
13		24–26	–12	188	17.1	379	2.9	1.6	17.4	5.0	ND	
14		26–30.1	–8	191	17.0	382	4.1	1.7	17.2	6.1	ND	
15	4 Mar 1999	3.7–12	–2	188	17.6	388	3.3	1.5	17.4	3.8	nvc	
16		12–14	–6	189	17.6	391	3.8	1.4	17.6	5.6	nvc	
17		14–18	–6	190	18.3	404	4.6	1.5	16.4	5.3	nvc	
18		18–21.6	–4	189	17.4	388	3.7	1.4	17.7	5.1	nvc	
19	6 Mar 1999	7–16	–11	189	16.8	377	3.2	3.5	16.8	3.2	nvc	
20		16–17.7	–18	195	17.1	393	8.4	3.7	17.3	9.8	nvc	
21		17.7–20	–18	194	16.6	382	7.0	3.6	18.2	15.1	nvc	
22		20–27	–6	191	16.6	375	3.8	2.6	17.1	5.2	nvc	
23	9 Mar 1999	3.9–6	–6	184	16.8	365	1.3	2.1	16.7	1.4	15.5	
24		6–11.2	–8	187	16.6	368	2.3	2.7	16.5	2.3	16.6	
25		11.2–14	–18	190	17.4	389	4.1	2.4	16.3	4.5	15.3	
26		14–15.8	–19	189	16.9	378	3.3	2.5	16.8	3.3	ND	
27		15.8–19	–15	188	17.4	385	3.1	2.3	16.6	3.3	14.1	
28		19–22.2	–10	188	16.5	368	2.4	2.3	17.1	3.9	16.6	
29	11 Mar 1999	9.5–20	–14	187	16.9	374	2.3	2.7	16.9	2.3	16.8	
30		20–21.2	–11	187	16.8	372	2.2	2.1	16.9	2.5	16.8	
31		21.2–23	–10	186	17.0	372	1.9	2.9	17.0	2.0	17.1	
32		23–24.2	–6	187	16.6	369	2.2	2.5	16.7	2.4	16.6	
33		24.2–27	–5	189	16.6	373	3.0	2.5	16.7	3.1	16.4	
34		27–31	–3	189	16.3	368	3.0	2.6	16.4	3.6	14.0	
35	15 Mar 1999	13–17	–3	186	17.0	372	1.8	2.9	17.0	1.8	ND	
36		22–25.5	10	190	16.1	366	3.3	2.5	16.9	6.1	ND	
37	16 Mar 1999	29–33	13	188	16.8	374	2.6	2.9	16.7	2.6		

^aAll the profiles were made in the longitude sector 48°E–60°E; more details, including plan views of flight paths, are available in the work of *Stefanutti et al.* [2004]. Abbreviations are as follows: UCSE, Unit for Connection of Scientific Equipment, which records aircraft parameters; Time, duration of flight segment, ks since 00Z; Lat, latitude, °N; T_{cp}, cold-point temperature, K; Z_{cp}, cold-point pressure-altitude, km; θ_{cp}, cold-point potential temperature, K; e_{cp}, cold-point saturation mixing ratio, ppmv; χ_H, hygropause water vapor mixing ratio, ppmv; Z_H, hygropause pressure-altitude, km; e_H, hygropause saturation mixing ratio, ppmv; Z_{CT}, cloud-top pressure-altitude for backscatter ratio > 2 at 532 nm; x, not reached; ND, no data; nvc, no cloud with backscatter ratio above 2 at 532 nm, observed.

and 200 ppbv ozone thresholds were found, in order to provide insight into the vertical structure of the TTL. Ozone mixing ratios around 100 ppbv have been used in the extratropics to define the “chemical tropopause” [e.g., *Bethan et al.*, 1996]. The variation of these various tropopause-like quantities is displayed in Figure 1. The analysis to derive the lapse-rate tropopause in the aircraft profiles is somewhat subjective, since the ascent has a substantial horizontal component that can produce a noisy lapse-rate profile in the presence of even modest horizontal temperature gradients [*Danielsen*, 1993]. A 90 s running average was used to smooth the data in the lapse-rate calculation. The lapse-rate tropopause is generally lower than the cold-point tropopause, by up to 1 km for individual profiles, and by 500 m in the mean. The cold-point and the lapse-rate tropopause heights are only weakly correlated ($r^2 = 0.53$).

Reid and Gage [1996] found that the monthly mean lapse-rate tropopause at Truk (7.5°N, 151.8°E) for 1980 was 150 m below the monthly mean cold point.

[20] In the TTL, the ozone profile often contains a local maximum, or even several local maxima. The lowest altitude, at which an ozone mixing ratio of 100 ppbv was observed during APE-THESEO, varies from 13.3 to 17.6 km (mean: 16.1 km, or 373 K potential temperature). This altitude is usually located over a kilometer beneath the cold point tropopause and varies independently of the cold-point tropopause ($r^2 = 0.06$), as also found by *Folkens et al.* [1999]. The highest altitudes with an ozone mixing ratio of 100 ppbv are located closer to the cold-point tropopause (13.4 to 18.1 km, mean: 16.7 km, or 377 K potential temperature (Figure 1)), but are also not correlated ($r^2 = 0.06$). In several profiles, even ozone mixing ratios of 200 ppbv were found below the cold point. These high ozone values indicate ongoing ozone production during the slow ascent of air in the TTL [*Folkens et al.*, 1999] and/or transport from the stratosphere into the TTL as suggested by *Tuck et al.* [1997, 2004]. The highest altitude with a 200 ppbv ozone mixing ratio (16.8–18.7 km, mean: 17.7 km, or 398 K potential temperature) shows a relatively strong positive correlation with the cold-point tropopause ($r^2 = 0.64$). This suggests that the highest altitude at which a 200 ppbv ozone mixing ratio occurs is in the lower stratosphere, aligned with a potential temperature surface. The good correlation between cold point and the highest altitude with a 200 ppbv ozone mixing ratio implies that much of the observed variability of the tropopause height in Figure 1 is associated with reversible wave motion.

[21] Figure 2 shows the potential temperature of the cold-point tropopause, the hygropause, and the range of potential temperatures for which each profile was saturated with respect to water ice. The tropopause and hygropause data are given with respect to pressure-altitude in Table 1. From Figures 1 and 2 and Table 1, we can deduce the following. In the deep tropics in the Indian Ocean, i.e., latitudes equatorward of 20°, the cold-point tropopauses observed vary in temperature and height from 194 K at 16.6 km to 182 K at 18.1 km. There was variation in the observed cold-point potential temperature from 365 K to 404 K. The mean of the cold-point temperatures is 188 K, at a mean potential temperature of 380 K. As will be discussed further below, the cold point and hygropause can be rather poorly defined sometimes, due to small vertical gradients in temperature and water vapor (or total water). However, taking the data in Figure 2 at face value, 11 profiles show the hygropause at a potential temperature more than 5 K above the tropopause, 5 show the hygropause more than 5 K below the tropopause, and 21 show the tropopause and hygropause within 5 K of each other. There is neither a clear and consistent setting of the tropopause and hygropause to the same altitude by dehydration processes, nor a clear and consistent separation of tropopause and hygropause by the Brewer-Dobson circulation. Of the 37 profiles, 6 are saturated at the tropopause but not at the hygropause, none are saturated at the hygropause but not at the tropopause, and 13 are saturated at both the tropopause and hygropause. Eleven profiles are saturated to potential temperatures more than 5 K above the hygropause. This variability of saturation conditions at the hygropause and tropopause underlines the

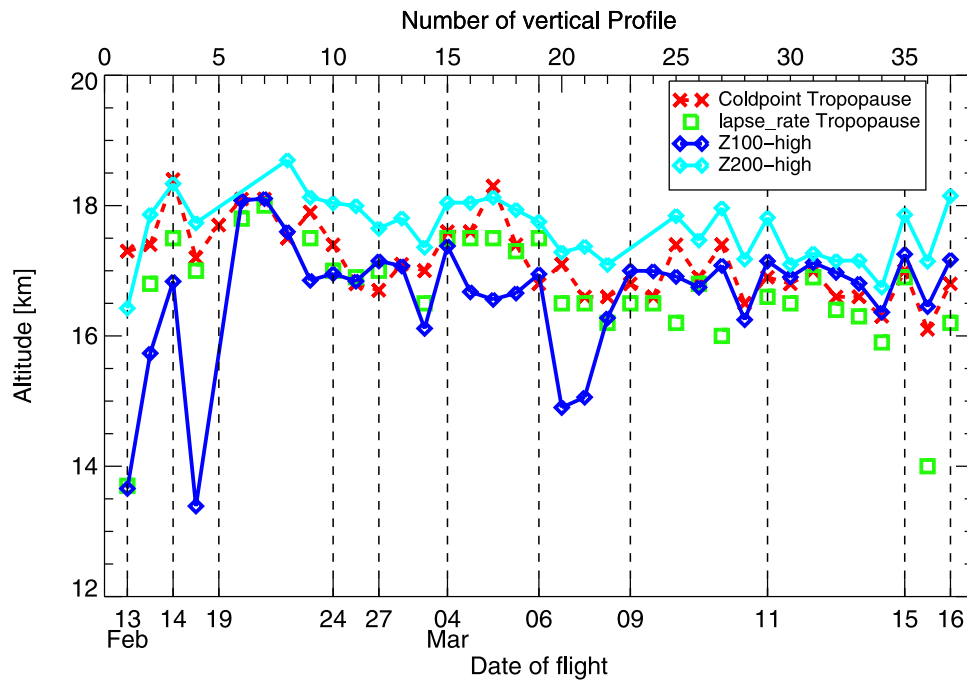


Figure 1. Cold-point tropopause (crosses), lapse-rate tropopause (squares), and the highest pressure-altitudes where 100 and 200 ppbv ozone thresholds were found (diamonds) for all tropical ascents and descents of the APE-THESEO campaign. Profile numbers are as in Table 1.

complex processes occurring during the observation period. Neither the tropopause nor the hygropause provide a location where conditions consistently approach those implied by a simple “stratospheric fountain” hypothesis (i.e., a high frequency of cloud and saturation with

subsaturation above and below), and where simple deductions of water vapor mixing ratios could be made from temperature soundings.

[22] Figure 3 shows the total water as measured by FISH, saturation water vapor mixing ratio (with respect to ice) and

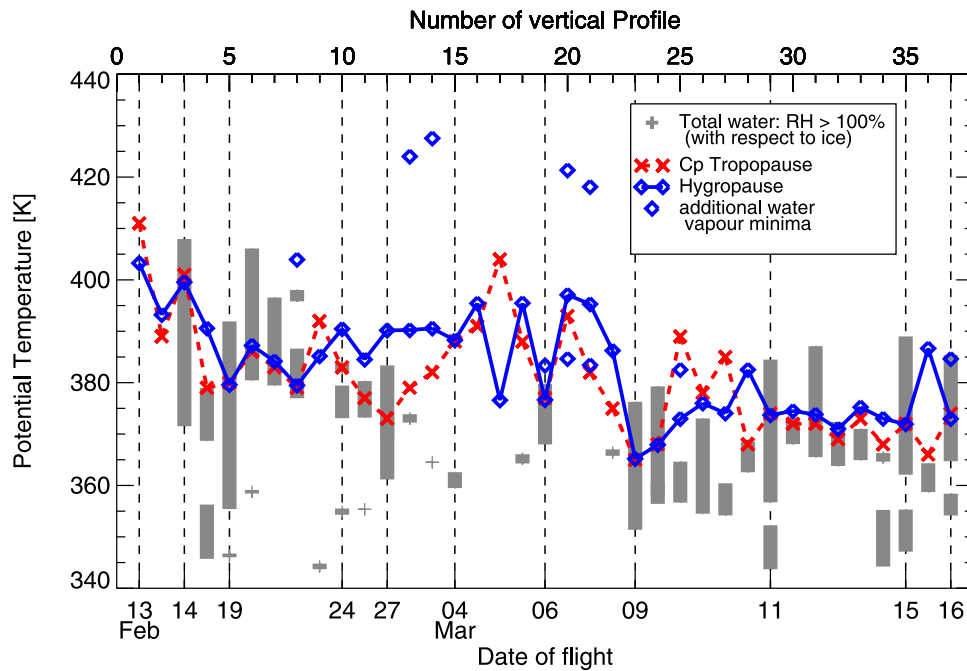


Figure 2. Potential temperature of the cold-point tropopause (crosses) and the hygropause (i.e., the minimum measured total water by FISH) (diamonds) for each ascent and descent of the *Geophysica* across the hygropause. Additional minima in total water are shown as diamonds. Also shown is the section of each profile that is saturated with respect to water ice (shaded bars).

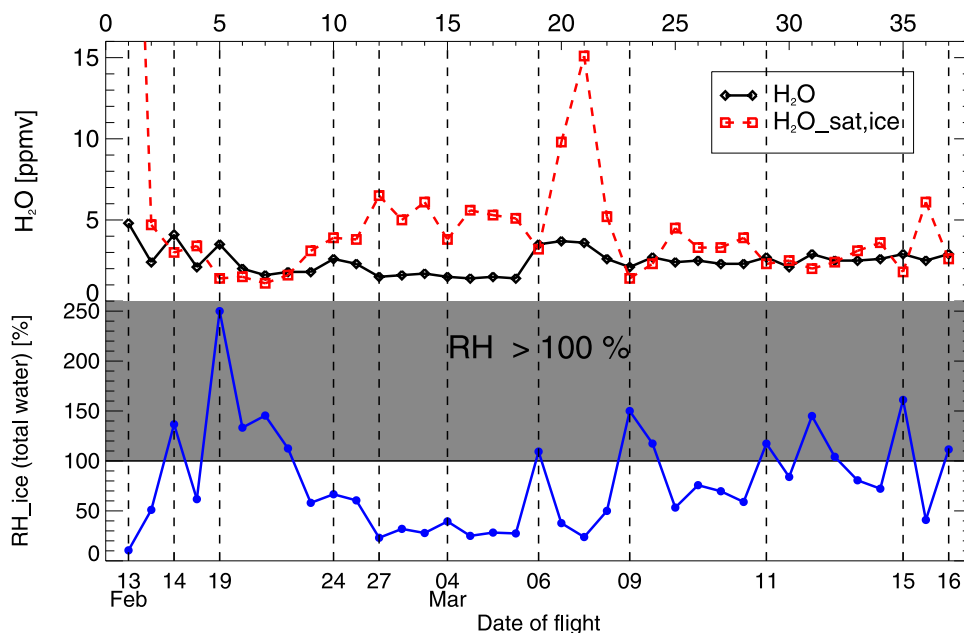


Figure 3. (top) Total water mixing ratio (diamonds) and saturated vapor mixing ratio over ice (squares) at the hygropause for each ascent and descent of the *Geophysica* across the hygropause. The profiles are the same as those listed in Table 1. (bottom) Relative humidity (RH) over water ice at the hygropause for each ascent and descent of the *Geophysica* across the hygropause. The region above 100% RH is shaded.

relative humidity (for total water) at the hygropause for each ascent and descent. The hygropause total water mixing ratios, measured by FISH, range from 1.4 to 4.1 ppmv. The mean hygropause total water mixing ratios is 2.4 ppmv, at a mean pressure altitude of 17.2 km (383 K potential temperature).

[23] Also shown in Table 1 are cloud-top pressure-altitudes for clouds above 14 km and a 532 nm backscatter ratio greater than 2, as derived from MAS measurements. This backscatter ratio threshold for cloudiness will miss ultrathin cirrus clouds (UTTCs), which were frequently observed during APE-THESEO. The 532 nm backscatter ratio for UTTCs is about 1.2 only [Peter *et al.*, 2003; Luo *et al.*, 2003a, 2003b]. Detection of such thin clouds is not usually possible from MAS data alone, and is outside the scope of the present discussion. The statistics below on cloud occurrence are, therefore, lower limits. Seventeen of the vertical profiles show clouds, 8 show no clouds, and 12 have no cloud data available. When clouds are present with backscatter ratio greater than 2, cloud-top pressure-altitudes range from 14 km to 18.1 km. 10 of the 17 vertical profiles with clouds have cloud tops within 200 m of the cold point.

[24] The distributions of values around the mean for most of the parameters in Table 1 are generally near-normal, given the small sample ($n \leq 37$). The distributions of saturation mixing ratios are lognormal, as expected from the exponential dependence of the saturation mixing ratio on temperature.

4. Discussion

4.1. Individual Profiles: Clouds, Water Vapor, and Meteorological Conditions

[25] Examples of specific vertical profiles of water, ozone, clouds and temperature measured during APE-THESEO are discussed in this section. They include two cases involving

cirrus clouds whose characteristics, origin and impact on the water vapor budget are investigated. The third and fourth profiles are clear-sky profiles, demonstrating the vertical structure of the TTL over the Indian Ocean without the direct influence of clouds. Profiles are numbered as per Table 1.

4.1.1. Profile 29: 11 March 1999

[26] The first example has relatively thick (but still barely visible) cirrus clouds at the tropopause, and a relatively low cold-point potential temperature. Figure 4 shows the lidar cross section through this cloud along the flight path of the

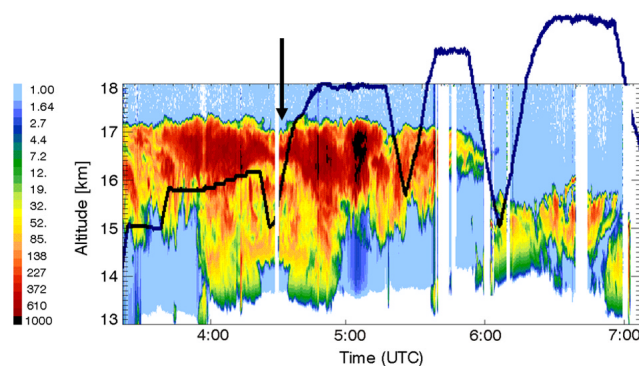


Figure 4. Backscatter ratio (ratio of air plus aerosol to air molecular backscatter intensity) at 1064 nm of the cirrus cloud on 11 March 1999, measured by the lidar on board the *Falcon* aircraft approximately 1 hour prior to the *Geophysica* observations; the *Geophysica* flight track is given by the blue line. The *Falcon* turned back at 0430 at 14°S; hence the symmetry in the cirrus about the turn point. The aspect ratio is 1:250, i.e., the cloud structures are compressed horizontally by a factor of 250. The vertical profile shown in Figure 5 is marked by the arrow.

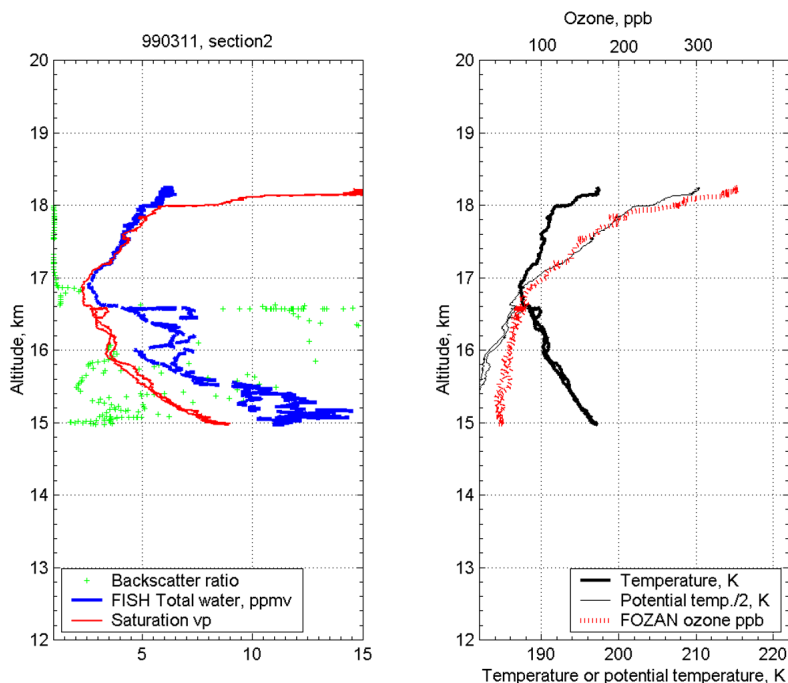


Figure 5. Vertical profiles from an ascent near 14°S on 11 March 1999. (left) Multiwavelength Aerosol Laser Scatterometer (MAS) backscatter ratio at 532 nm, FISH total water (ppmv), and saturation vapor mixing ratio (ppmv). Note that MAS data extend off-scale. The maximum backscatter recorded by MAS on the flight leg was 48, at an altitude of 16.6 km. (right) Temperature (K), potential temperature (K), and FOZAN ozone mixing ratio (ppbv). The potential temperature data have been divided by two for ease of plotting.

Falcon, which was obtained approximately 1 hour before in situ measurements from the *Geophysica* were made. The vertical extent of this cloud varied between 1 and 4 km with a cloud top around 17.2 km.

[27] The cirrus cloud in Figure 4 was profiled by the *Geophysica* at different locations about 1 hour after the *Falcon* measurements (the flight path is overlaid on the lidar curtain plot). The individual profiles, i.e., the vertical extension of the cirrus, are consistent in both measurements. As an example, Figure 5 shows a profile from 11 March 1999 (profile 29 in Table 1, marked by an arrow in Figure 4). The hygro-pause is at 16.9 km ($\theta = 374$ K), and occurs at the top of a cloud, as indicated by the backscatter data. Consistent with the lidar data, the cloud at the hygro-pause is relatively thick geometrically and optically, indicative of a (barely) visible cirrus cloud: backscatter ratios, at 532 nm, often exceed a value of 10. The condensed water mixing ratios, calculated as the difference of total water measurement of FISH and the saturation mixing ratio, are up to 3.5 ppmv. Total water mixing ratios of 7–8 ppmv above 16 km are significantly higher than in clear-sky profiles during APE-THESEO and thus a clear indicator for injection of water from lower altitudes. The cold-point tropopause is coincident with the hygro-pause. There is a stable and saturated layer, of several hundred meters, above the cold point. This layer is free of cloud. At the top of the saturated layer, the gradient of the ozone profile increases significantly. In the core of the clouds, however, ozone values are only 50–70 ppbv and thus significantly lower than observed elsewhere in the TTL (see below).

[28] The other profiles on 11 March, but also those of 9 March (12 profiles in all), have very similar characteristics: barely visible cirrus of more than 1 km vertical extension, with ice water content up to 6 ppmv, and cloud top and hygro-pause close to the rather low tropopause. Ozone mixing ratios of 50–70 ppbv were measured in the clouds of these profiles which are significantly lower than their environment and do not show the increase of ozone usually observed in the TTL [e.g., *Folkins et al.*, 1999]. These air masses are therefore likely transported rapidly from lower altitudes probably in convective systems [see also *Sherwood and Dessler*, 2000].

[29] Meteosat 5 images combined with wind analysis (Figure 6) imply that these clouds were likely to be the direct result of convective cloud outflow. Several hours before the airborne observations, cloud top temperatures of less than 193 K (-80°C) were observed east of the southern part of the flight track in several extended convective cells. Cloud top temperatures below 193 K in these days, corresponding to a pressure altitude of 100 hPa, were among the lowest observed in the APE-THESEO period over the Indian Ocean, when convection usually did not exceed 16 km [*Stefanutti et al.*, 2004]. Wind velocities at 100 hPa were easterly and about 30 m s^{-1} (UKMO output, not shown), and so allow the outflow from these systems to be transported in 4 to 12 hours to the region of the flight track (as sketched in Figure 6). To estimate the radiative effect of the cirrus cloud, the heating rate has been calculated, based on the actual observations of O_3 , H_2O , and cloud extinction and following the method of *Corti et al.*

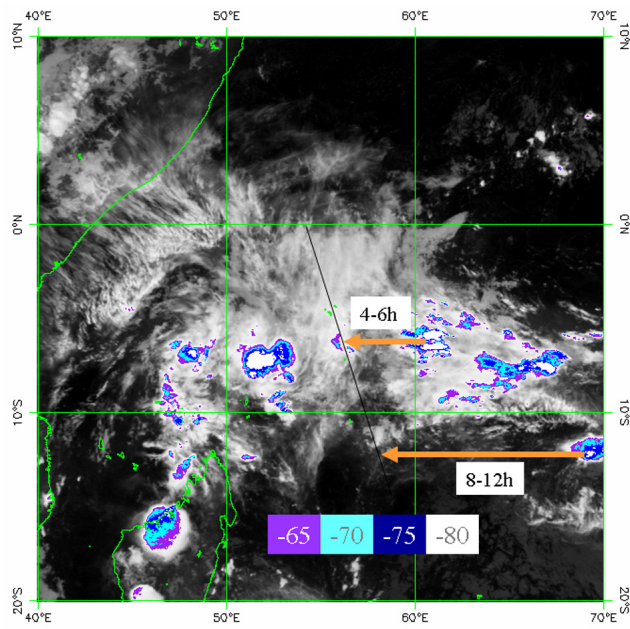


Figure 6. Meteosat 5 infrared cloud image, 5 hours (0116 LT, 2116 GMT) prior to the takeoff of the *Geophysica* aircraft from the Seychelles (green islands in the center of the plot) on 11 March 1999. The flight path is given as the black line. The aircraft first flew south-southeastward, then returned along the track north-northwestward, overflew Mahé, reached the equator, and then returned south-southeastward. Colors indicate cloud-top height in degrees Celsius (see legend bar). Orange arrows show the transport of recently convected air at 100 hPa in the time intervals shown.

[2005]. Mean heating rates for the cloud are from 12 to 18 K d⁻¹. With a vertical gradient in potential temperature of 10 K km⁻¹, the cloud could be lifted by several hundred meters on its way from the convective area to the observation region. Consistently, ECMWF analyses show rather high vertical transport velocities in the area of the cirrus cloud areas, of around 2 cm s⁻¹. The cloud-radiation interaction at least compensates for cloud particle sedimentation, which, for particles with radii of 15–20 μm, is similar in magnitude to the rate of cloud lofting.

[30] Figure 7 (solid lines) shows the frequency distribution of relative humidity over ice (RH_i) for the profiles of the flight on 11 March. Outside clouds, RH_i usually does not exceed 50%, peaking at 20% and is thus not close to saturation conditions to form new cirrus. In the clouds themselves, the RH_i distribution peaks at 100% with only a few observations of moderate supersaturation. This suggests that the clouds in Figures 4 and 5 are “aged” to near-equilibrium conditions or already in the process of evaporation, which corroborates the finding that they originate directly from convective activity and were transported to the position of the observation.

4.1.2. Profile 6: 19 February 1999

[31] Figure 8 shows a profile measured on 19 February 1999. The hygro-pause is at 18.1 km ($\theta = 387$ K), and occurs toward the top of a cloud, as indicated by the backscatter data. The cloud at the hygro-pause is relatively thin: back-

scatter ratios are less than 10, and condensed water mixing ratios are below 3 ppmv. *Santacesaria et al.* [2003] have analyzed this case, and calculated optical depths on or slightly above the threshold for visibility for different parts of the cloud field around the sounding shown in Figure 8. The cold-point tropopause is coincident with the hygro-pause. There is a saturated, near-adiabatic layer above the cold point, with potential temperature increasing much more slowly between 18 km and 18.5 km than above or below. The backscatter data at this altitude are noisy, but show no clear signs of a cloud. Ozone mixing ratios are between 70 ppbv and 100 ppbv for altitudes above 16.9 km, i.e., from well below the cold point.

[32] The profile shown in Figure 8, with very tenuous subvisible cirrus clouds near the tropopause and a relatively high cold-point potential temperature, is similar to all those observed on 19 February. In the absence of strong convection near the flight path, the observed cooling and cloud condensation must be due to processes other than convection, such as gravity or planetary waves. While convection reaching the tropopause was not frequent during the APE-THESIO period, less energetic convection, capable of generating gravity waves, was widespread [*Stefanutti et al.*, 2004]. A mechanism for the formation of the profile shown in Figure 8 is discussed in detail by *Santacesaria et al.* [2003]; a related example, but with direct injection of water by convection into a cloud originally formed above convection, is discussed by *Garrett et al.* [2004]. Trajectory calculations place the air observed on 19 February over convection less than 24 hours previously. Gravity wave–

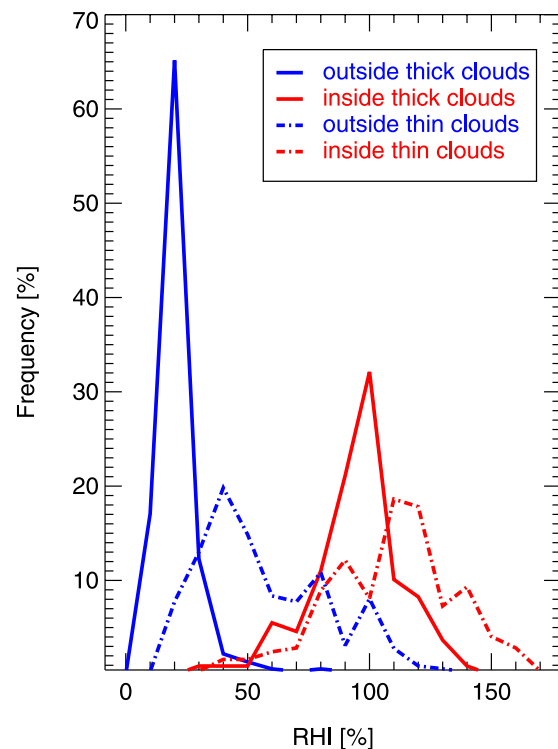


Figure 7. Frequency distribution of relative humidity as measured by FLASH on the flight on 11 March 1999 (solid lines) and on 19 February 1999 (dashed lines), separated for observations inside (red) and outside (blue) clouds.

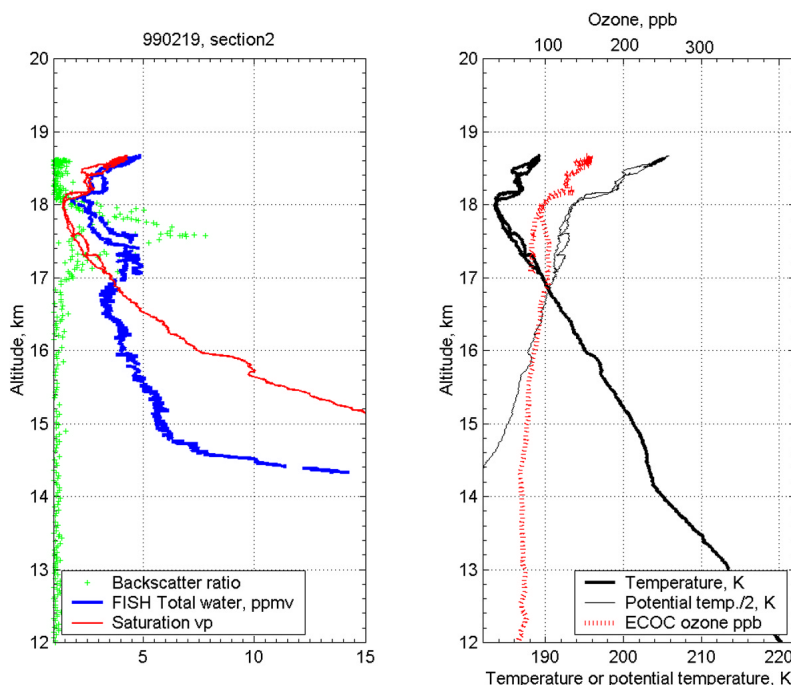


Figure 8. Vertical profiles from a descent near the equator on 19 February 1999. (left) MAS backscatter ratio at 532 nm, FISH total water (ppmv), and saturation vapor mixing ratio (ppmv). (right) Temperature (K), potential temperature (K), and Electro-Chemical Ozone Cell (ECOC) ozone mixing ratio (ppbv). The potential temperature data have been divided by two for ease of plotting.

induced turbulence above the convection probably initiated the transport of water to the cold point. On subsequent cooling, this transported water vapor condensed to form a subvisible cirrus. The UTTCs reported by *Peter et al.* [2003] and *Luo et al.* [2003a, 2003b] (e.g., profile 12 in Table 1) occur in profiles similar to that shown in Figure 8 and might originate from these subvisible cirrus clouds. Ozone mixing ratios are close to 100 ppbv (Figure 8) which is a typical TTL value and thus significantly higher compared to the profile in Figure 5 discussed above. This makes a recent direct injection of lower tropospheric air unlikely.

[33] The corresponding frequency distributions of RH_i on 19 February (Figure 7, dashed lines) are different than for 11 March. Outside clouds, much higher humidity is observed, including supersaturated air up to 130%. Inside the cirrus, also a higher fraction of air is supersaturated up to RH_i = 170%, i.e., further from equilibrium. This could suggest that a smaller fraction of their growth timescale has elapsed since nucleation compared to the fraction elapsed in the thicker clouds. Since the thick, anvil outflow, cirrus have number densities about 1 order of magnitude larger than the thin cirrus [*Thomas et al.*, 2002], the growth timescale of the thin clouds will be one order of magnitude longer for the thin clouds (i.e., 100 s compared to 10 s [see, e.g., *Kärcher and Lohmann*, 2002]), observations of the thin clouds far from equilibrium will be more frequent. Further, the coldest temperatures on 11 March were 185–190 K and thus the cloud among the coldest ever observed. Under these conditions, supersaturation can be maintained even for hours. The cloud might then have gone through several warming and cooling cycles due to changing temperatures, which change the relative humidity significantly, but not necessarily

the absolute amount of water vapor. The findings support the idea that these thin clouds close to the tropopause are unlikely to originate from the direct outflow of convection.

[34] Both types of clouds affect the water budget of their environment in a different way: the thick cloud (Figures 4, 5, and 7) carries additional water into the TTL and is thus likely moistening the ambient air. However, the thin cloud close to the tropopause, in Figures 8 and 7, which is formed in situ by local cooling in air masses close to saturation, has a greater chance of dehydrating the air to the local saturation water vapor mixing ratio, as discussed by *Luo et al.* [2003b].

4.1.3. Profile 19: 6 March 1999

[35] Figure 9 shows a profile from 6 March 1999 (profile 19 in Table 1). The hygro-pause is not well pronounced: there is a broad region (16.5–17.6 km) with mixing ratios below 4 ppmv, which is a much higher value than for the previously discussed profiles; the actual total water minimum is at 16.8 km. The cold-point tropopause is coincident with the hygro-pause (16.8 km, $\theta = 377$ K) and occurs at the top of a moderately stable layer (lapse rate approximately 6 K km^{-1}), extending from a shallow inversion at 13.1 km. There is a marked increase in stability above the cold point, but a 500 m thick neutral layer occurs between 17.1 and 17.6 km. In the TTL, the water vapor mixing ratio is between 4 and 10 ppmv, the ozone mixing ratio is close to 50 ppbv, and the backscatter ratio near unity, i.e., no clouds (including UTTCs) are detected. Convective clouds with cloud-top temperatures above -65°C were present below the aircraft during this part of the flight and there are indications of small-scale waves that may have been induced by the convection, as discussed by *Stefanutti et al.* [2004], especially their Figures 7 and 11.

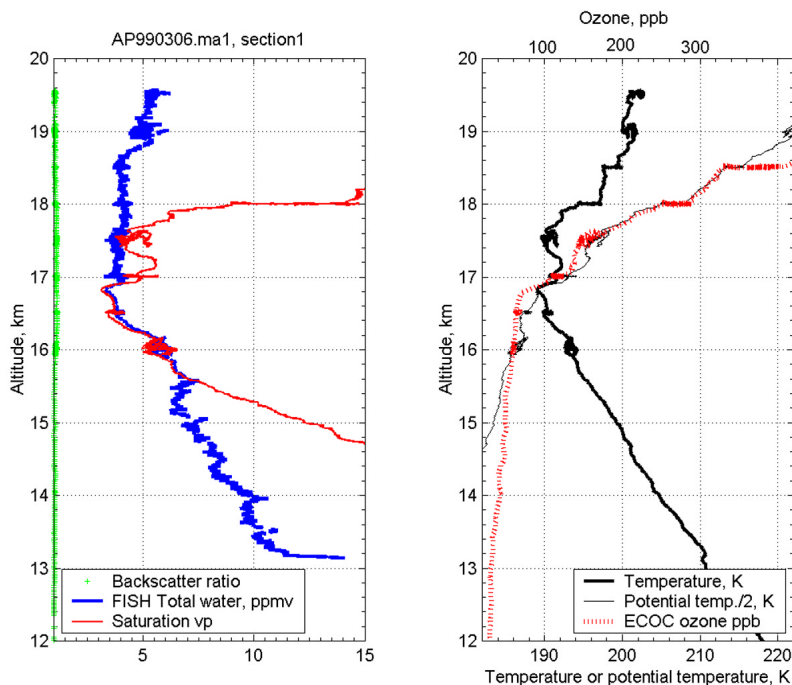


Figure 9. Vertical profiles from an ascent near 11°S on 6 March 1999. (left) MAS backscatter ratio at 532 nm, FISH total water (ppmv), and saturation vapor mixing ratio (ppmv). (right) Temperature (K), potential temperature (K), and ECOC ozone mixing ratio (ppbv). The potential temperature data have been divided by two for ease of plotting.

[36] There are two regions of water vapor saturation in the profile shown in Figure 9: between 15.7 km and the cold point, and between 17.3 and 17.6 km (although there are a range of temperatures, and hence saturation mixing ratios for the portion of the flight near 17.5 km, the time series of data (not shown) demonstrate that there are periods of saturation). The coincidence of cold point, hygropause, and saturation indicates that the tropopause-level water vapor mixing ratio in this profile could be correctly deduced from a temperature-only sounding (e.g., a radiosonde), but the lack of cloud in the profile indicates that no dehydration is occurring at this place and time. However, since the profile is saturated near the tropopause, the water vapor mixing ratio might have been “set” by the local temperatures just recently before the observation.

4.1.4. Profile 21: 6 March 1999

[37] Figure 10 shows a profile from 6 March 1999 (profile 21 in Table 1). The hygropause is not well pronounced: there is a broad region with mixing ratios below 4 ppmv which is a much higher value than for the first two example profiles, the actual minimum being at 18.2 km. The cold-point tropopause is at 16.6 km ($\theta = 382$ K), and occurs at the base of a broad (1 km deep) layer of cold temperatures. Above this layer there are two further near-adiabatic layers producing secondary temperature minima, each minimum matching features in the total water profile, including the hygropause at 18.2 km. In the TTL, the water vapor mixing ratio is between 4 and 8 ppmv, the ozone mixing ratio is close to 100 ppbv, and the backscatter ratio near unity, i.e., no clouds (including UTTCs) are detected.

[38] In the cloud-free profile shown in Figure 10, multiple maxima/minima can be identified in the temperature, water

vapor, and ozone profiles, and there is no simple relation between cold point, hygropause, and cloud top. These multiple maxima/minima may be due to differential advection of air that has experienced different degrees of dehydration, or may be due to the production of mixed layers when gravity waves reach their critical levels [Teitelbaum *et al.*, 1999]. This type of profile could also be the result of projecting aircraft data from a sloping vertical travel into the height-temperature and height-water vapor planes, in which case the water vapor and ozone layers are indicative of mesoscale horizontal variations in the tropopause and hygropause height. However, since we are concerned with the large-scale ascent of air into the stratosphere, it does not matter greatly whether we consider these features to be directly on top of each other or not. Similar profiles were observed on 4 March, 15 March, and at other times on 6 March. The frequent occurrence of such profiles, which have no simple relationship between the temperature and water vapor profiles, questions the usefulness of applying a simple dehydration hypothesis to all vertical temperature soundings through the tropical tropopause region.

4.2. General View of the Tropopause Transition Layer Above the Indian Ocean in Early 1999

[39] Out of 36 profiles during APE-THESEO, 7 show cold point, hygropause, and cloud top within 200 m of each other. A further five profiles show cold point and hygropause within 200 m of each other, but no clouds at that altitude. Two further profiles show cold point and cloud top within 200 m of each other. The frequent coincidence of cold point and hygropause suggests that dehydration is occurring, or has just occurred, in situ at the cold point

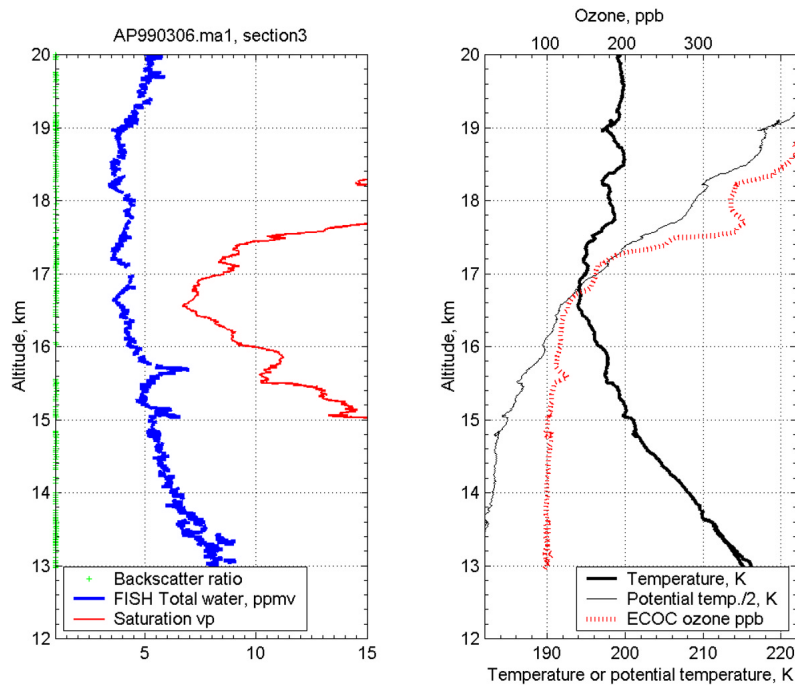


Figure 10. Vertical profiles from an ascent near 18°S on 6 March 1999. (left) MAS backscatter ratio at 532 nm, FISH total water (ppmv), and saturation vapor mixing ratio (ppmv). (right) Temperature (K), potential temperature (K), and ECOC ozone mixing ratio (ppbv). The potential temperature data have been divided by two for ease of plotting.

over the Indian Ocean. The observations of clouds at the cold point, as indicated by FISH measurements, MAS measurements (Table 1), and other measurements aboard the *Geophysica* and from the *Falcon* [Thomas *et al.*, 2002; Santacesaria *et al.*, 2003], support this view.

[40] Comparison with radiosonde measurements across the equatorial Indian Ocean show that the *Geophysica* data are consistent with the radiosonde data, and that the high, cold tropopause seen during APE-THESEO is representative of the entire region (Table 2). The tropopause temperatures observed by the *Geophysica* correspond to a mean saturation water vapor pressure of 3.0 ppmv. However, the mean measured hygropause mixing ratio was even lower, at 2.4 ppmv. This discrepancy with the mean saturation mixing ratio is due to the large number of unsaturated profiles. This clearly demonstrates that discussions of tropical tropo-

sphere-stratosphere dehydration and entry-level water should not be based solely on instantaneous temperature analyses [Vömel and Oltmans, 1999].

[41] As expected for the season of APE-THESEO, the mean H₂O mixing ratios at the tropopause are below the averaged “entry level” of stratospheric water vapor mixing ratios estimated from stratospheric measurements of water vapor and methane [e.g., Dessler and Kim, 1999, and references therein]. Figure 11 compares the range of APE-THESEO total water profiles with those from previous missions. Diagrams of this kind have been presented as evidence of the operation of the tropical “tape recorder” (i.e., the upward transport of relatively isolated tropical air by the Brewer-Dobson circulation [Mote *et al.*, 1996]). In the profile from Darwin in January–February 1987 [Kelly *et al.*, 1993], the mean hygropause, shown in Figure 11,

Table 2. Monthly Mean Cold Points and Cold-Point Potential Temperatures During 1999 for Stations Across the Indian Ocean

Station	Location	Cold-Point Temperature, K				Potential Temperature of Cold Point, ^a K				Number of Ascents to Pressures <100 mbar			
		Dec	Jan	Feb	Mar	Dec	Jan	Feb	Mar	Dec	Jan	Feb	Mar
<i>West Indian Ocean</i>													
Kenya	17°S, 39°23'E		191	185	188		368	382	382		33	35	7
Serge-Frolow	15°20'S, 54°20'E	191	193	190	190	388	372	398	382	22	27	27	29
Seychelles	4°42'S, 55°30'E	189	189	187	189	392	388	382	388	28	59	54	56
Mauritius ^b	20°11'S, 57°20'E	198	197	192	196	382	378	378	378	17	16	17	20
<i>East Indian Ocean</i>													
Cocos Islands	12°S, 97°E	189	189	187	188	378	382	382	362	38	36	41	38
Sumatra	0°30'S, 100°12'E	186	187	186	191	398	392	392	392	11	16	41	54

^aCold-point potential temperatures are for the midpoint of 5 K potential temperature bins.

^bNo ascents above 390 K are recorded in the database.

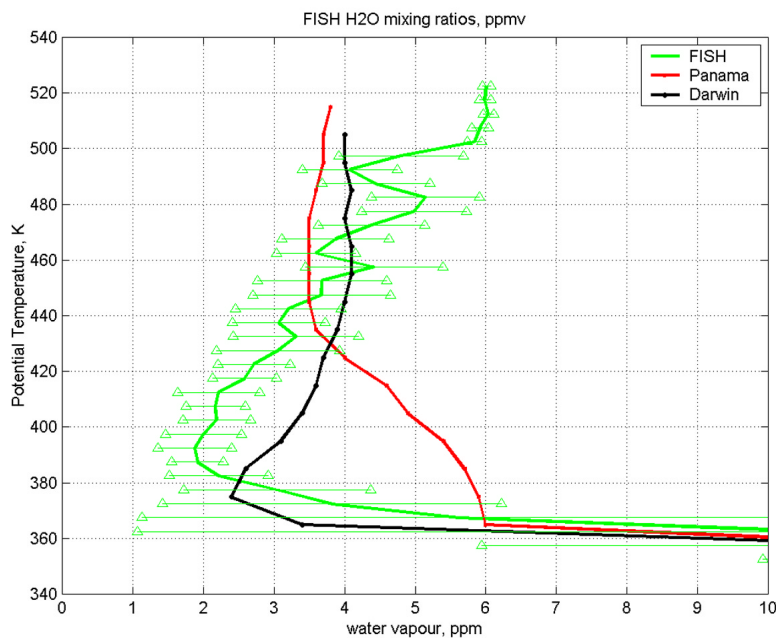


Figure 11. A comparison of the range of water vapor profile from FISH (February–March 1999) with profiles from Darwin [Kelly *et al.*, 1993], which took place in January and February 1987, and Panama [Kley *et al.*, 1982], which took place in September 1980. The range bars on the FISH data show ± 1 standard deviation.

coincides with the mean tropopause. In the profile from Panama in September 1980 [Kley *et al.*, 1982], the hygropause occurs at potential temperatures about 100 K above the tropopause. The data from APE-THESEO show a broad minimum, at potential temperatures about 20 K higher than the Darwin minimum, but, like the Darwin minimum, coincident with the mean tropopause. Since we have presented evidence above for the occurrence of dehydration at potential temperatures above 370 K, passive (nondehydrating) vertical advection by the “tape recorder” is not the only mechanism determining the water vapor profile, for potential temperatures between 370 K and 400 K (i.e., above 17.5 km). The Darwin and APE-THESEO profiles have a similar shape between 390 K and 470 K, although the data from APE-THESEO are lower than the Darwin data. However, Vömel *et al.* [1995] also report for the same season (but for the Central Pacific Ocean) single profiles with water vapor mixing ratios at the hygropause of less than 1.5 ppmv.

[42] As a whole, the results show the western equatorial Indian Ocean to be a site of active dehydration during northern winter/spring 1999. Comparing our results to the climatology of Newell and Gould-Stewart [1981], a number of possibilities arise. In this climatology, localized regions with high frequencies of monthly mean 100 mbar temperatures of -82.4°C or below were found. In Northern Hemisphere summer, these localized regions were the Indian and SE Asian monsoon regions. In Northern Hemisphere winter, the localized region was the western Pacific Ocean, with “an extension of this low-temperature area into the Indian Ocean and over to Africa albeit with lower frequency” [Newell and Gould-Stewart, 1981]. APE-THESEO may have been fortunate to sample such a less frequent active dehydration period in the western Indian

Ocean [cf. Newell and Gould-Stewart, 1981, Figure 2]. Bonazzola and Haynes [2004] and Fueglistaler and Haynes [2005] show, based on ECMWF operational analysis data and ERA-40 data, respectively, that the APE-THESEO period was indeed characterized by lower tropopause temperatures over the western Pacific Ocean and the Indian Ocean region than, for example, the period December 1997 to February 1998. The mean entry-level water vapor mixing ratio across the tropics reported by Fueglistaler and Haynes [2005] is 2.2 ppmv, which agrees well with the mean hygropause total water mixing ratios of 2.4 ppmv as derived from our measurements, while those of the previous year are higher by approximately 1 ppmv [Bonazzola and Haynes, 2004]. Rather than APE-THESEO having sampled an anomalously cold year, another explanation could be that the Newell and Gould-Stewart climatology did not consider cold points at pressures below 100 hPa, and this may have significantly affected their analysis, since the higher mode in the distribution of measured cold-point potential temperatures occurs at a pressure of about 80 mbar. Or, last, the apparent cooling of the tropopause and stratosphere since 1979 [e.g., Simmons *et al.*, 1999] may have caused the area of the “stratospheric fountain” to spread.

5. Summary and Conclusions

[43] APE-THESEO made in situ measurements of ozone, water vapor, total water, and cloud properties above the western equatorial Indian Ocean in February and March 1999. We have combined measurements of temperature, total water, water vapor, clear-sky relative humidity, and cloud to show evidence of active dehydration as air is transported from troposphere to stratosphere. The tropopause, as indicated by the temperature minimum or “cold

point,” was high (i.e., a mean pressure-altitude of 17 km, equivalent to a potential temperature of 380 K) and cold (i.e., 190 K (-83°C) in the mean). The mean measured water vapor minimum (i.e., the hygropause) was 2.4 ppmv, at a mean altitude close to the mean cold-point altitude. The mean saturation water vapor mixing ratio does not accurately represent the mean of the measured water vapor mixing ratios, since the air was unsaturated in the region of the cold point for about 40% of the measurements. The very low mixing ratios observed during APE-THESEO are comparable to those found in previous studies in the “fountain region” over Micronesia.

[44] The lapse-rate tropopause, although difficult to determine from aircraft data, was generally lower than the cold point, rather than at the same altitude as would be the case for radiative-convective adjustment [Thuburn and Craig, 2002]. The highest altitude of 100 ppbv ozone mixing ratios was also generally lower than the cold point. Clouds were observed up to the altitude of the cold point. We identified cirrus clouds with differing characteristics: first, visible or just subvisible cirrus clouds at relatively low potential temperatures, which stem from the direct outflow of anvils (with subsequent advection and lofting), and second, subvisible cirrus and ultrathin cirrus occurring at higher potential temperatures. These latter clouds are triggered either by vertical motion of air above convective systems or wave activity in the TTL, but are not directly linked to the outflow of cumulonimbus clouds, which do not often reach these altitudes over the Indian Ocean. The different origins of the two classes of clouds are indicated by the different frequency distributions of relative humidity (both inside and outside of the clouds) for each class. While the first class of clouds injected from the outflow of anvils into the dry TTL will moisten its environment, the second class of cirrus has the potential for effective dehydration of the air masses.

[45] In single events, ongoing dehydration was observed in air parcels at potential temperatures as high as 390 K. Ongoing dehydration at potential temperatures this high will smear out the zonal mean “tape recorder” signal. Water vapor profiles from different regions of active dehydration, when plotted against potential temperature, will have minima at different potential temperatures (between 370 K and 400 K) and only above 400 K will passive vertical advection of the water vapor minimum by the Brewer-Dobson circulation dominate everywhere. Detailed transport studies are required to decide whether air passes through multiple active (i.e., dehydrating) cold points between 370 K and 400 K. Initial studies [Bonazzola and Haynes, 2004] suggest that transport through the layer between 360 K and 380 K is relatively localized, but that horizontal transport in the layer does bring air parcels through the coldest regions. In summary, the data from APE-THESEO demonstrate the complicated behavior of water vapor, clouds, and ozone in the region of the tropical tropopause. The TTL over the western equatorial Indian Ocean was found to be a region with active dehydration down to very low water vapor mixing ratios, acting on air masses before they reach the stratosphere.

[46] **Acknowledgments.** The authors gratefully acknowledge the help and advice of their APE-THESEO colleagues, including S. Borrmann, R. Carla, K. S. Carslaw, D. Lowe, B. P. Luo, P. Mazzino, V. Mitev,

O. Riediger, G. Toci, and M. Volk. We would like to thank the pilots and ground crew of the M55 *Geophysica* for the flexible and safe operation of the aircraft in a very difficult environment. This work was carried out as part of EC contract ENV4 CT97 0533, NERC contract GST/02/2210, NERC contract NER/T/S/2000/00977, and BMBF contract 01 LA 9829/3 within the program “Angewandte Klima- und Atmosphärenforschung,” with funding from the Italian Space Agency (ASI) and with help in kind from the U.K. Met Office. The authors are grateful to the Seychelles Directorate of Civil Aviation for substantial help with mission logistics. Paul Berrisford, of the U.K. Universities’ Global Atmospheric Modeling Programme, and the British Atmospheric Data Centre provided ERA climatologies, for which we thank them.

References

- Adriani, A., F. Cairo, M. Viterbini, S. Mandolini, L. Pulvirenti, and G. DiDonfrancesco (1999), Multiwavelength Aerosol Scatterometer for airborne experiments to study the optical properties of stratospheric aerosol, *J. Atmos. Oceanic Technol.*, *16*, 1329–1336.
- Bethan, S., G. Vaughan, and S. J. Reid (1996), A comparison of ozone and thermal tropopause heights and the impact of tropopause definition on quantifying the ozone content of the troposphere, *Q. J. R. Meteorol. Soc.*, *122*, 929–944.
- Beuermann, J. (2000), Einfluss von Transportprozessen auf die Wasserdampfverteilung in der Tropopausenregion, Ph.D. thesis, Univ. of Bonn, Germany.
- Bonazzola, M., and P. H. Haynes (2004), A trajectory-based study of the tropical tropopause region, *J. Geophys. Res.*, *109*, D20112, doi:10.1029/2003JD004356.
- Brewer, A. W. (1949), Evidence for a world circulation provided by the measurements of helium and water vapour distribution in the stratosphere, *Q. J. R. Meteorol. Soc.*, *75*, 351–363.
- Corti, T., B. P. Luo, T. Peter, H. Vömel, and Q. Fu (2005), Mean radiative energy balance and vertical mass fluxes in the equatorial upper troposphere and lower stratosphere, *Geophys. Res. Lett.*, *32*, L06802, doi:10.1029/2004GL021889.
- Danielsen, E. F. (1982), A dehydration mechanism for the stratosphere, *Geophys. Res. Lett.*, *9*, 605–608.
- Danielsen, E. F. (1993), In situ evidence of rapid, vertical, irreversible transport of lower tropospheric air into the lower tropical stratosphere, *J. Geophys. Res.*, *98*, 8665–8681.
- Dessler, A. E., and H. Kim (1999), Determination of the amount of water vapor entering the stratosphere based on Halogen Occultation Experiment (HALOE) data, *J. Geophys. Res.*, *104*, 30,605–30,607.
- Dethof, A., A. O’Neill, and J. Slingo (2000), Quantification of the isentropic mass transport across the dynamical tropopause, *J. Geophys. Res.*, *105*, 12,279–12,293.
- Dvortsov, V. L., and S. Solomon (2001), Response of the stratospheric temperatures and ozone to past and future increases in stratospheric humidity, *J. Geophys. Res.*, *106*, 7505–7514.
- Flentje, H., A. Dörnbrack, A. Fix, A. Meister, H. Schmid, S. Füglistaler, B. P. Luo, and T. Peter (2002), Denitrification inside the stratospheric vortex in the winter of 1999–2000 by sedimentation of large nitric acid trihydrate particles, *J. Geophys. Res.*, *107*(D16), 4314, doi:10.1029/2001JD001015.
- Folkins, I., M. Loewenstein, J. Podolske, S. J. Oltmans, and M. Proffitt (1999), A barrier to vertical mixing at 14 km in the tropics: Evidence from ozonesondes and aircraft measurements, *J. Geophys. Res.*, *104*, 22,095–22,102.
- Forster, P. M. de F., and K. P. Shine (1999), Stratospheric water vapor changes as a possible contributor to observed stratospheric cooling, *Geophys. Res. Lett.*, *26*, 3309–3312.
- Fueglistaler, S., and P. H. Haynes (2005), Control of interannual and longer-term variability of stratospheric water vapor, *J. Geophys. Res.*, *110*, D24108, doi:10.1029/2005JD006019.
- Fueglistaler, S., H. Wernli, and T. Peter (2004), Tropical troposphere-to-stratosphere transport inferred from trajectory calculations, *J. Geophys. Res.*, *109*, D03108, doi:10.1029/2003JD004069.
- Fueglistaler, S., M. Bonazzola, P. H. Haynes, and T. Peter (2005), Stratospheric water vapor predicted from the Lagrangian temperature history of air entering the stratosphere in the tropics, *J. Geophys. Res.*, *110*, D08107, doi:10.1029/2004JD005516.
- Garrett, T. J., A. J. Heymsfield, M. J. McGill, B. A. Ridley, D. G. Baumgardner, T. P. Bui, and C. R. Webster (2004), Convective generation of cirrus near the tropopause, *J. Geophys. Res.*, *109*, D21203, doi:10.1029/2004JD004952.
- Highwood, E., and B. J. Hoskins (1998), The tropical tropopause, *Q. J. R. Meteorol. Soc.*, *124*, 1579–1604.
- Holton, J. R., and A. Gettelman (2001), Horizontal transport and the dehydration of the stratosphere, *Geophys. Res. Lett.*, *28*, 2799–2802.

- Holton, J. R., P. H. Haynes, M. E. McIntyre, A. Douglass, R. Rood, and L. Pfister (1995), Stratosphere-troposphere exchange, *Rev. Geophys.*, **33**, 403–439.
- Jensen, E., O. B. Toon, L. Pfister, and H. B. Selkirk (1996), Dehydration of the upper troposphere and lower stratosphere by subvisible cirrus clouds near the tropical tropopause, *Geophys. Res. Lett.*, **23**, 825–828.
- Kärcher, B., and U. Lohmann (2002), A parameterization of cirrus cloud formation: Homogeneous freezing of supercooled aerosols, *J. Geophys. Res.*, **107**(D2), 4010, doi:10.1029/2001JD000470.
- Kelly, K. K., M. H. Proffitt, K. R. Chan, M. Loewenstein, J. R. Podolske, S. E. Strahan, J. C. Wilson, and D. Kley (1993), Water vapor and cloud water measurements over Darwin during the STEP 1987 tropical mission, *J. Geophys. Res.*, **98**, 8713–8723.
- Kley, D., A. L. Schmeltekopf, K. Kelly, R. H. Winkler, T. L. Thompson, and M. MacFarland (1982), Transport of water through the tropical tropopause, *Geophys. Res. Lett.*, **9**, 617–620.
- Kley, D., J. Russell III, and C. Phillips (Eds.) (2000), SPARC assessment of UT/S water vapour, *Rep. WCRP-113, WMO/TD 1043, SPARC 2*, Dep. of Phys., Univ. of Toronto, Toronto, Ont., Canada.
- Kyrö, E., et al. (2000), Ozone measurements during the Airborne Polar Experiment: Aircraft instrument validation; isentropic trends; and hemispheric fields prior to the 1997 Arctic ozone depletion, *J. Geophys. Res.*, **105**, 14,599–14,611.
- Luo, B. P., et al. (2003a), Ultrathin Tropical Tropopause Clouds (UTTCS): II. Stabilisation mechanisms, *Atmos. Chem. Phys.*, **3**, 1093–1100.
- Luo, B. P., et al. (2003b), Dehydration potential of ultrathin clouds at the tropical tropopause, *Geophys. Res. Lett.*, **30**(11), 1557, doi:10.1029/2002GL016737.
- MacKenzie, A. R., V. Santacesaria, A. Adriani, V. Yushkov, S. Balestri, C. Kiemle, and L. Stefanutti (2000), APE-THESEO: Clouds, dehydration, and transport at the tropical tropopause, *SPARC Newsl.*, **14**, 18–21.
- Merkulov, S., and V. Yushkov (1999), Some results of aircraft stratospheric water vapor measurement in the arctic polar vortex (in Russian), *Meteorol. Hydrol.*, **7**, 107–113.
- Mote, P. W., K. H. Rosenlof, M. E. McIntyre, E. S. Carr, J. C. Gille, J. R. Holton, J. S. Kinnerson, H. C. Pumphrey, J. M. Russell, and J. W. Waters (1996), An atmospheric tape recorder: The imprint of tropical tropopause temperatures on stratospheric water vapor, *J. Geophys. Res.*, **101**, 3989–4006.
- Newell, R., and S. Gould-Stewart (1981), A stratospheric fountain?, *J. Atmos. Sci.*, **38**, 2789–2796.
- Peter, T., et al. (2003), Ultrathin Tropical Tropopause Clouds (UTTCS): I. Cloud morphology and occurrence, *Atmos. Chem. Phys.*, **3**, 1083–1091.
- Potter, B. E., and J. R. Holton (1995), The role of monsoon convection in the dehydration of the lower tropical stratosphere, *J. Atmos. Sci.*, **52**, 1034–1050.
- Reid, G. C., and K. S. Gage (1996), The tropical tropopause over the western Pacific: Wave-driving, convection, and the annual cycle, *J. Geophys. Res.*, **101**, 21,233–21,241.
- Rosenlof, K. H., et al. (2001), Stratospheric water vapor increases of the past half-century, *Geophys. Res. Lett.*, **28**, 1195–1198.
- Santacesaria, V., et al. (2003), Clouds at the tropical tropopause: A case study during the APE-THESEO campaign over the western Indian Ocean, *J. Geophys. Res.*, **108**(D2), 4044, doi:10.1029/2002JD002166.
- Schiller, C., et al. (1999), Ice particle formation and sedimentation in the tropopause region: A case study based on in-situ measurements of total water during POLSTAR1997, *Geophys. Res. Lett.*, **26**, 2219–2222.
- Sherwood, S. C., and A. E. Dessler (2000), On the control of stratospheric humidity, *Geophys. Res. Lett.*, **27**, 2513–2516.
- Simmons, A. J., A. Untch, C. Jakob, P. Källberg, and P. Undén (1999), Stratospheric water vapour and tropical tropopause temperatures in ECMWF analyses and multi-year simulations, *Q. J. R. Meteorol. Soc.*, **125**, 353–386.
- Stefanutti, L., L. Sokolov, A. R. MacKenzie, S. Balestri, and V. Khatatov (1999), The M-55 Geophysica as a platform for the Airborne Polar Experiment, *J. Atmos. Oceanic Technol.*, **16**, 1303–1312.
- Stefanutti, L., et al. (2004), The APE-THESEO tropical campaign: An overview, *J. Atmos. Chem.*, **48**, 1–33, doi:10.1023/B:JOCH.0000034509.11746.b8.
- Teitelbaum, H., M. Moustou, R. Sadourmy, and F. Lott (1999), Critical levels and mixing layers induced by convectively generated gravity waves during CEPEX, *Q. J. R. Meteorol. Soc.*, **125A**, 1715–1734.
- Thomas, A., et al. (2002), In situ measurements of background aerosol and subvisible cirrus in the tropical tropopause region, *J. Geophys. Res.*, **107**(D24), 4763, doi:10.1029/2001JD001385.
- Thuburn, J., and G. C. Craig (2002), On the temperature structure of the tropical stratosphere, *J. Geophys. Res.*, **107**(D2), 4017, doi:10.1029/2001JD000448.
- Tuck, A. F., et al. (1997), The Brewer-Dobson circulation in the light of high altitude in situ aircraft observations, *Q. J. R. Meteorol. Soc.*, **124**, 1–70.
- Tuck, A. F., et al. (2004), Horizontal variability 1–2 km below the tropical tropopause, *J. Geophys. Res.*, **109**, D05310, doi:10.1029/2003JD003942.
- Vömel, H., and S. J. Oltmans (1999), Comment on “A reexamination of the ‘stratospheric fountain’ hypothesis” by A. E. Dessler, *Geophys. Res. Lett.*, **26**, 2737–2738.
- Vömel, H., S. J. Oltmans, D. Kley, and P. J. Crutzen (1995), New evidence for the stratospheric dehydration mechanism in the equatorial Pacific, *Geophys. Res. Lett.*, **22**, 3235–3238.
- Vömel, H., et al. (2002), Balloon-borne observations of water vapor and ozone in the tropical upper troposphere and lower stratosphere, *J. Geophys. Res.*, **107**(D14), 4210, doi:10.1029/2001JD000707.
- Wang, P. H., et al. (1996), A 6-year climatology of cloud occurrence frequency from Stratospheric Aerosol and Gas Experiment II observations (1985–1990), *J. Geophys. Res.*, **101**, 29,407–29,430.
- Yushkov, V., A. Oulanovsky, N. Lechenuk, I. Roudakov, K. Arshinov, F. Tikhonov, L. Stefanutti, F. Ravegnani, U. Bonafé, and T. Georgiadis (1999), A Chemiluminescent Analyzer for Stratospheric Measurements of the Ozone Concentration (FOZAN), *J. Atmos. Oceanic Technol.*, **16**, 1345–1350.
- Zöger, M., C. Schiller, and N. Eicke (1999), Fast in-situ hygrometers: A new family of balloon-borne and airborne Lyman α photofragment fluorescence hygrometers, *J. Geophys. Res.*, **104**, 1807–1816.

A. Adriani, Istituto di Fisica dello Spazio Interplanetario, Consiglio Nazionale delle Ricerche, via del Fosso del Cavaliere, 100, I-00133 Roma, Italy.

J. Beuermann, Eurofins Hamburg, Geierstrasse 1, D-22305 Hamburg, Germany.

O. Bujok, VDI Technologiezentrum, Graf-Recke-Str. 84, D-40239 Düsseldorf, Germany.

F. Cairo, Istituto di Scienze dell’Atmosfera e del Clima, Sezione di Roma, Consiglio Nazionale delle Ricerche, Via Fosso del Cavaliere 100, I-00133 Roma, Italy.

T. Corti and T. Peter, Institute for Atmospheric and Climate Science, Swiss Federal Institute of Technology, Universitätsstrasse 16, CHN 012.1, CH-8092 Zürich, Switzerland.

G. DiDonfrancesco, Ente per le Nuove Tecnologie, l’Energia, e l’Ambiente, Via Anguillarese 301, Santa Maria di Galeria, I-00060 Roma, Italy.

I. Gensch, M. Krämer, S. Rohs, and C. Schiller, Institute for Stratospheric Research, Forschungszentrum Jülich GmbH, Jülich D-52425, Germany.

C. Kiemle, Deutsches Zentrum für Luft- und Raumfahrt Oberpfaffenhofen, IPA, Oberpfaffenhofen, D-82234 Wessling, Germany.

C. Kröger, National Isotope Centre Institute of Geological and Nuclear Sciences, PO Box 31312, Lower Hutt, New Zealand.

A. R. MacKenzie, Environmental Science Department, Lancaster University, Lancaster LA1 4YQ, UK. (r.mackenzie@lancaster.ac.uk)

S. Merkulov, A. Oulanovsky, V. Rudakov, and V. Yushkov, Central Aerological Observatory, 141700, Dolgoprudny, Moscow Region, Pervomayskaya 3, Russia.

F. Ravegnani, Istituto di Scienze dell’Atmosfera e del Clima, Consiglio Nazionale delle Ricerche, Via Gobetti, 101, I-40129 Bologna, Italy.

P. Salter, 31 Old Wokingham Road, Crowthorne RG45 6SS, UK.

V. Santacesaria, Advanced Computer Systems, SpA, Via Della Bufalotta 378, I-00139 Roma, Italy.

L. Stefanutti, Geophysica-GEIE, Via Pancaldo 21, I-50127 Firenze, Italy.